

Electromagnetic Emission Rates and Spectral Sum Rules *

James Steele^a Hidenaga Yamagishi^b and Ismail Zahed^c

^aDepartment of Physics, The Ohio State University, Columbus, OH 43210, USA

^b4 Chome 11-16-502, Shimomeguro, Meguro, Tokyo, Japan. 153.

^cDepartment of Physics, SUNY, Stony Brook, New York 11794, USA

The electromagnetic emission rates at SPS energies satisfy spectral constraints in leading order in the pion and nucleon densities. These constraints follow from the strictures of broken chiral symmetry. We saturate these constraints using available data, leading to model independent emission rates from a hadronic gas. With a simple fire-ball scenario, only large nucleon densities may account for the present CERES data.

1. Recent relativistic heavy-ion collisions at CERN have reported an excess of dileptons over a broad range of lepton invariant mass [1,2]. A possible excess was also reported in the direct photon spectrum [3]. In this talk, we would like to show that under the assumption that the heavy-ion collision at SPS energies trigger a hadronic gas, the photon and dilepton emission rates are constrained by available data in the vacuum, to leading order in the pion and the nucleon density. The density expansion is justified if we note that in the hadronic gas the expansion parameters are $\kappa_\pi = n_\pi/2m_\pi f_\pi^2 \lesssim 0.3$ for the pions, and $\kappa_N = n_N g_A^2/2m_N f_\pi^2 \lesssim 0.3$ for nucleon densities $n_N \lesssim 3\rho_0$ with $\rho_0 \sim 0.17 \text{ fm}^{-3}$ the nuclear matter density [4].

2. In a hadronic gas in thermal equilibrium, the rate \mathbf{R} of dileptons produced in an unit four volume follows from the thermal expectation value of the electromagnetic current-current correlation function [5]. For massless leptons with momenta p_1, p_2 , the rate per unit invariant momentum $q = p_1 + p_2$ is given by

$$\frac{d\mathbf{R}}{d^4q} = -\frac{\alpha^2}{6\pi^3 q^2} \frac{2}{1 + e^{q^0/T}} \text{Im} \mathbf{W}^F(q) \quad (1)$$

where $\alpha = e^2/4\pi$ is the fine structure constant, and

$$\mathbf{W}^F(q) = i \int d^4x e^{iq \cdot x} \text{Tr} \left(e^{-(\mathbf{H} - \mu \mathbf{N} - \Omega)/T} T^* \mathbf{J}^\mu(x) \mathbf{J}_\mu(0) \right).$$

$e\mathbf{J}_\mu$ is the hadronic part of the electromagnetic current, \mathbf{H} is the hadronic Hamiltonian, μ the baryon chemical potential, \mathbf{N} the baryon number operator, Ω the Gibbs energy, T the temperature, and the trace is over a complete set of hadron states.

*Work supported by the Department of Energy under grant No. DE-FG-88ER40388

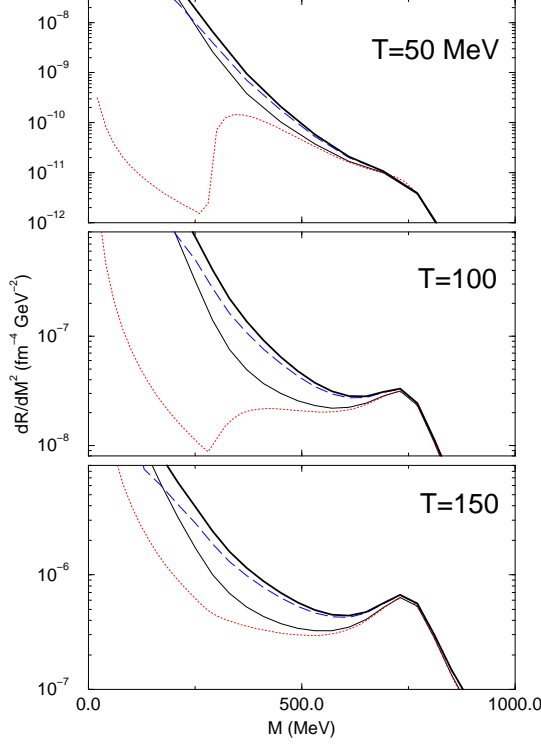


Figure 1. The dielectron rate for pions alone (dotted), pions and Δ (solid), and pions and one-loop (dashed). The contribution from pions, Δ , and one-loop together is represented by the thick solid line. A fixed nucleon density of ρ_0 was used.

3. For temperatures $T \lesssim m_\pi$ and baryonic densities $n_N \lesssim 3\rho_0$ we may expand the trace in (2) using pion and nucleon states. To first order in the density, we have

$$\text{Im } \mathbf{W}^F(q) = -3q^2 \text{Im } \mathbf{\Pi}_V(q^2) + \frac{1}{f_\pi^2} \int d\pi \mathbf{W}_\pi^F(q, k) + \int dN \mathbf{W}_N^F(q, p) + \mathcal{O}(\kappa_\pi^2, \kappa_N^2, \kappa_\pi \kappa_N). \quad (2)$$

The phase space factors are

$$dN = \frac{d^3p}{(2\pi)^3} \frac{1}{2E_p} \frac{1}{e^{(E_p - \mu)/T} + 1} \quad \text{and} \quad d\pi = \frac{d^3k}{(2\pi)^3} \frac{1}{2\omega_k} \frac{1}{e^{\omega_k/T} - 1}$$

with the nucleon energy $E_p = \sqrt{m_N^2 + p^2}$ and the pion energy $\omega_k = \sqrt{m_\pi^2 + k^2}$. The first term in (2) is the transverse part of the isovector correlator $\langle 0 | T^* \mathbf{V} \mathbf{V} | 0 \rangle$ and summarises the results of the resonance gas model. It is given by the e^+e^- annihilation data. At low q^2 it is dominated by the ρ, ρ', \dots , while at high q^2 its tail is dual to the $q\bar{q}$ spectrum.

The term linear in pion density can be reduced by the use of chiral reduction formulas to a form amenable to experimental determinations. The important contributions are [6]

$$\begin{aligned} \mathbf{W}_\pi^F(q, k) \simeq & \quad 12q^2 \text{Im } \mathbf{\Pi}_V(q^2) - 6(k+q)^2 \text{Im } \mathbf{\Pi}_A((k+q)^2) + (q \rightarrow -q) \\ & + 8((k \cdot q)^2 - m_\pi^2 q^2) \text{Im } \mathbf{\Pi}_V(q^2) \times \text{Re}(\Delta_R(k+q) + \Delta_R(k-q)) \end{aligned} \quad (3)$$

with $\Delta_R(k)$ the retarded pion propagator, and Π_A the transverse part of the isoaxial correlator $\langle 0|T^*\mathbf{j}_A\mathbf{j}_A|0\rangle$ which follows from tau decay data [6]. It is dominated by the a_1 resonance.

The term linear in the nucleon density is just the spin-averaged forward Compton scattering amplitude on the nucleon with virtual photons. This is only measured for various values of $q^2 \leq 0$. However, the dilepton and photon rates require $q^2 \geq 0$. Therefore, only the photon rate for this term can be determined directly from data by use of the optical theorem

$$e^2 \mathbf{W}_N^F(q, p) = -4(s - m_N^2) \sum_I \sigma_{\text{tot.}}^{\gamma N}(s) \quad (4)$$

with $s = (p + q)^2$. For off-shell photons, we must resort to chiral constraints to determine the nucleon contribution to the dilepton rate. Broken chiral symmetry dictates uniquely the form of the strong interaction Lagrangian (at tree level) for spin $\frac{1}{2}$. Perturbative unitarity follows from an on-shell loop-expansion in $1/f_\pi$, that enforces current conservation and crossing symmetry. To one-loop the contribution in this case is parameter free. The large contribution of the Δ to the Compton amplitude near threshold is readily taken into account by adding it as a unitarized tree term to the one-loop result [4].

Our dilepton rate at $T = 150\text{MeV}$ is shown in Fig. 1. The dominant effect in our case comes from the continuum and not the Δ resonance. At $M = 400\text{ MeV}$, the inclusion of nucleons enhances the rate by a factor of three. Others who have taken nucleons into account through various methods [7] find enhancements in the rate similar to our result. In our calculations there is no shift of the dilepton pair production ρ peak.

4. In order to fully understand the role of the experimental cuts, we have used a simple fire-ball evolution. The details of these calculations are given in [4]. The results are shown in fig. 2, for S-Au and Pb-Au collisions. The Dalitz and prompt omega decays were borrowed from the transport model [8]. Adding the nucleon contribution gives the solid line in fig. 2. The effect of the cuts is dramatic, resulting in a very small enhancement. Only if we take the extreme case of the baryon density totally saturated by nucleons do we start to reach the lower error bars of the data in the $M = 200 - 400\text{ MeV}$ regime as shown by the dashed-dotted line. The large πN enhancement noted in the rate calculation in fig. 1 is not present because the temperature dies away quickly, thereby decreasing the nucleon density and rate dramatically. The fast depletion of baryons in time is also noted in realistic cascade and hydrodynamical evolutions.

We can also evolve the photon rates and compare with the upper bounds set by WA80 for S-Au[3]. The inclusion of nucleons put the rate right on the edge of the upper limit for the data [4], in the fire ball scenario. Since we have analyzed both the dilepton and photon rates simultaneously, this implies that more enhancement of the dilepton rate would overshoot the photon data, a particularly important point in our analysis.

5. For temperatures $T \sim m_\pi$ and densities $\rho \leq 3\rho_0$, we may treat a hadronic gas as dilute, and organize the various emission rates using a density expansion. Assuming that the heavy-ion collisions at SPS energies release enough entropy in the form of hadronic constituents, to form a hadronic gas in the center of mass, we may assess reliably the photon and dilepton emission rates. To leading order in the density, the rates are constrained by data and general principles. With nucleon densities presently quoted for the

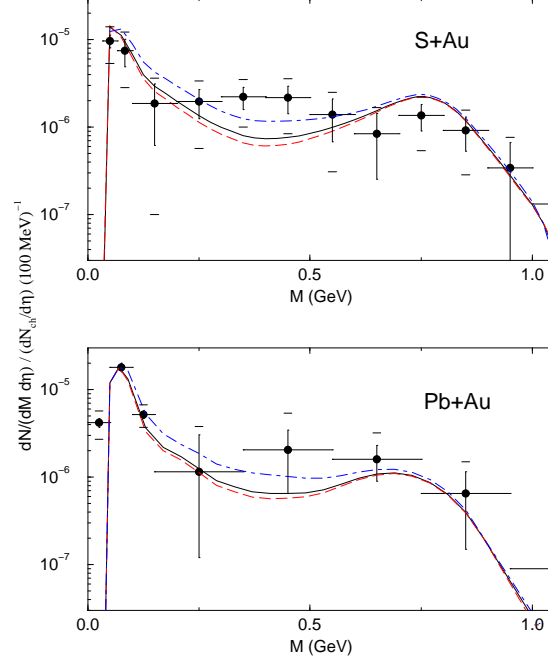


Figure 2. Our dielectron rate including the Δ and one-loop contributions evolved in space-time as in [4] for S-Au and Pb-Au collisions. In the upper graph, $n_N = 0, 0.7\rho_0$, and $2.5\rho_0$ are plotted as the dashed, solid, and dashed-dotted lines respectively. In the lower graph, the lines are for $n_N = 0, \rho_0$, and $4\rho_0$. The data are from [1]. The systematic errors are added linearly to the statistical error bars to give the cross line.

SPS experiments, we are not able to account for the present CERES data. Only larger nucleon densities (by about a factor of 4) may account for the data. We have checked that our results are not modified by next-to-leading order corrections in the densities [4]. It is important to note that our construction is not a model. Rather, models should agree with our analysis to leading order in the pion and nucleon densities. This construction can be extended to the higher mass region [9].

REFERENCES

1. G. Agakichiev, *et al.*, Phys. Rev. Lett. **75** (1995) 1272; Nucl. Phys. **A610** (1996) 317c.
2. M. Masera for the HELIOS-3 Collaboration, Nucl. Phys. **A590** (1995) 93c.
3. R. Santo *et al.*, Nucl. Phys. **A566** (1994) 61c; R. Albrecht *et al.*, Nucl. Phys. **A590** (1995) 81c.
4. J.V. Steele, H. Yamagishi, and I. Zahed, Phys. Rev. **D56** (1997) 5605.
5. L.D. McLerran and T. Toimela, Phys. Rev. **D31** (1985) 545; H.A. Weldon, Phys. Rev. **D42** (1990) 2384.
6. J.V. Steele, H. Yamagishi, and I. Zahed, Phys. Lett. **B384** (1997) 255.
7. R. Rapp, G. Chanfray, and J. Wambach, Nucl. Phys. **A617** (1997) 472; F. Klingl and W. Weise, Nucl. Phys. **A606** (1996) 329; F. Klingl, N. Kaiser, and W. Weise, Nucl. Phys. **A624** (1997) 527.
8. G.Q. Li, C.M. Ko, and G.E. Brown, Nucl. Phys. **A606** (1996) 568.
9. C.H. Lee, H. Yamagishi, and I. Zahed, In preparation.